Origins of Quasi-Biweekly and Intraseasonal Oscillations over the South China Sea and Bay of Bengal and Scale Selection of Unstable Equatorial and Off-Equatorial Modes

Ying ZHANG[1], Tim LI[2,3*], Jianyun GAO[4], and Wei WANG[5]

1 *Ningde Branch of Fujian Meteorological Bureau, China Meteorological Administration, Ningde* 352100, *China*
2 *Key Laboratory of Meteorological Disaster, Ministry of Education (KLME)/Joint International Research Laboratory of Climate and Environmental Change (ILCEC)/Collaborative Innovation Center on Forecast and Evaluation of Meteorological Disasters (CIC-FEMD), Nanjing University of Information Science & Technology, Nanjing* 210044, *China*
3 *Department of Atmospheric Sciences, School of Ocean and Earth Science and Technology, University of Hawaii, Honolulu, HI* 96822, *USA*
4 *Fujian Institute of Meteorological Sciences, China Meteorological Administration, Fuzhou* 350001, *China*
5 *Minhang District Office of Shanghai Meteorological Service, China Meteorological Administration, Shanghai* 201199, *China*

(Received July 12, 2019; in final form October 9, 2019)

ABSTRACT

The daily outgoing longwave radiation (OLR) field in boreal summer shows significant power spectrum peaks on quasi-biweekly (10–20-day) and intraseasonal (20–80-day) timescales over the Indo–western Pacific warm pool, especially over the South China Sea and Bay of Bengal. The quasi-biweekly oscillation (QBWO) originates from off-equatorial western North Pacific, and is characterized by a northwest–southeast oriented wave train pattern, propagating northwestward. The intraseasonal oscillation (ISO), on the other hand, originates from the equatorial Indian Ocean and propagates eastward and northward.

Why the equatorial mode possesses a 20–80-day periodicity while the off-equatorial mode favors a 10–20-day periodicity is investigated through idealized numerical experiments with a 2.5-layer atmospheric model. In the off-equatorial region, the model simulates, under a realistic three-dimensional summer mean flow, the most unstable mode that has a wave train pattern with a typical zonal wavelength of 6000 km and a period of 10–20 days, propagating northwestward. This is in contrast to the equatorial region, where a Madden–Julian oscillation (MJO) like mode with a planetary (wavenumber-1) zonal scale and a period ranging from 20 to 80 days is simulated. Sensitivity experiments with different initial conditions indicate that the QBWO is an intrinsic mode of the atmosphere in boreal summer in the off-equatorial Indo–western Pacific region under the summer mean state, while the MJO is the most unstable mode in the equatorial region.

Key words: quasi-biweekly oscillation (QBWO), intraseasonal oscillation (ISO), Madden–Julian oscillation (MJO), scale selection

Citation: Zhang, Y., T. Li, J. Y. Gao, et al., 2020: Origins of quasi-biweekly and intraseasonal oscillations over the South China Sea and Bay of Bengal and scale selection of unstable equatorial and off-equatorial modes. *J. Meteor. Res.*, **34**(1), 137–149, doi: 10.1007/s13351-020-9109-7.

1. Introduction

The Asian monsoon exhibits distinctive quasi-biweekly (10–20-day) and intraseasonal (20–80-day) oscillations in boreal summer (Murakami, 1980; Lau et al., 1988; Wang and Rui, 1990; Li et al., 2015; Xu et al., 2017; see Li and Wang, 2005; Li and Hsu, 2018 for a review on this subject). Xie et al. (1963) discovered a 40–50-day oscillation in zonal wind over the Indo–western Pacific sector (Li et al., 2018; Xie et al., 2018). Lau et al. (1988) found 40- and 20-day oscillations respectively in the rainfall field over East Asia and suggested that the former was associated with the Madden–Julian oscillation (Madden and Julian, 1971, 1972; hereafter

Supported by the National Key Research and Development Program of China (2018YFC1505805), US NOAA (NA18OAR4310298), US NSF (AGS-1643297), National Natural Science Foundation of China (41875069, 41575052, and 41575043), and Fund for Collaborative Innovation of Meteorological Science in East China (QYHZ201608). This is SOEST contribution number 10892, IPRC contribution number 1424, and ESMC number 298.

*Corresponding author: timli@hawaii.edu.

MJO) while the latter was affected by local processes. Chen et al. (2000) found power spectrum peaks at 30–60 and 12–24 days respectively in summer low-level zonal wind, equivalent black body temperature, and outgoing longwave radiation (OLR) fields over the South China Sea (SCS) and the Meiyu or Baiu front. Teng and Wang (2003) found dominant westward propagating signals on the quasi-biweekly timescale over the off-equatorial region and eastward propagating signals with around 50-day periodicity at the equator.

While many previous observational analyses revealed the marked oscillations on quasi-biweekly and intraseasonal timescales over the monsoon regions, the physical origins of the oscillations are unclear. In particular, for the quasi-biweekly oscillation (QBWO), although previous studies have illustrated their structure and propagation features (e.g., Hsu and Weng, 2001), dynamically what determines the preferred temporal and spatial scales is unclear. In contrast to an equatorially symmetric pattern in boreal spring (Wen et al., 2010), the QBWO shows a distinctive equatorially asymmetric structure in boreal summer. Goswami and Mathew (1994) suggested that the boreal summer QBWO is an intrinsic atmospheric mode excited by the evaporation–wind feedback in the presence of the monsoon westerly. In their theoretical study, however, an artificial time lag between convection and heating was required, in order to obtain an oscillatory solution. Chatterjee and Goswami (2004) proposed that the QBWO is an unstable $n = 1$ Rossby wave driven by the convective feedback in the presence of the equatorially asymmetric background mean flow.

The objective of the current study is to examine the origins of the QBWO and intraseasonal oscillation (ISO) of precipitation over the SCS and the Bay of Bengal (BoB), and to reveal the mechanism for spatial and temporal scale selection of the QBWO and ISO modes in the off-equatorial and equatorial regions, respectively. For the first objective, a diagnosis of observational data will be carried out. For the second objective, an intermediate atmospheric model will be applied for analysis in both the equatorial and off-equatorial regions.

The remaining part of this paper is organized as follows. In Section 2, the data and method are first introduced. This is followed by an observational data analysis of origins of the QBWO and ISO over the SCS and BoB in Section 3. In Section 4, we conduct a theoretical investigation of scale selection of the QBWO (ISO) mode in the off-equatorial (equatorial) region with an intermediate atmospheric model. Finally, conclusions and discussion are given in Section 5.

2. Data, method, and model

The primary observational data used in the current study include the NCEP/DOE (Department of Energy) Reanalysis II (Kanamitsu et al., 2002) and daily OLR product. Both datasets have a horizontal resolution of 2.5° × 2.5°. The analysis focuses on extended summer season (i.e., from May to October) for the period of 1979–2001.

A lagged correlation analysis is employed, with a reference box over the SCS (10°–20°N, 110°–120°E) and BoB (10°–20°N, 85°–95°E) respectively, to derive the structure and evolution features of the QBWO and ISO modes. Propagation vectors are calculated at each grid point based on the maximum lagged correlation coefficient in the surrounding region within a short time window (which is 2 days for the QBWO mode and 5 days for the ISO mode).

In addition to the lagged correlation analysis, a multivariate empirical orthogonal function (EOF) analysis is performed onto the bandpass filtered 850-hPa wind and vorticity fields over the Asian monsoon domain (10°S–30°N, 50°E–180°). Based on the leading EOF modes, a composite analysis is further applied to the 850-hPa wind and vorticity fields to reveal the spatial structure and evolution characteristics of the two modes.

A 2.5-layer atmospheric model (Li and Wang, 1994; Wang and Li, 1994; Wang and Xie, 1997; Jiang et al., 2004) is used to investigate the most unstable mode in the off-equatorial region in boreal summer. This model consists of two-level free atmosphere and a well-mixed planetary boundary layer (PBL). This model is essentially the same as that used previously in studying the planetary zonal scale selection of the equatorial mode at the equator (Li and Zhou, 2009; Li, 2014). The model has a horizontal resolution of 5° longitudes by 2° latitudes and covers the domain of 40°S–40°N, 0°–360°.

The governing equations are linearized based on either an idealized or realistic background mean state. The perturbation condensational heating in the middle troposphere (Q'_{m}) depends on both the vertically integrated mean and anomalous moisture convergences,

$$Q'_{\mathrm{m}} = \delta_1 Q_{\mathrm{m}} - \delta_2 \bar{Q}_{\mathrm{m}}, \tag{1}$$

where Q_{m} represents the total heating,

$$Q_{\mathrm{m}} = \frac{bL_{\mathrm{c}}}{\Delta p}[-(\omega'_{\mathrm{m}} + \bar{\omega}_{\mathrm{m}}) \times (\bar{q}_2 - \bar{q}_1) - (\omega'_{\mathrm{e}} + \bar{\omega}_{\mathrm{e}}) \times (\bar{q}_{\mathrm{e}} - \bar{q}_2)], \tag{2}$$

and $\bar{Q}_{\mathrm{m}}$ represents the heating due to the basic-state circulation,

$$\bar{Q}_{\mathrm{m}} = \frac{bL_{\mathrm{c}}}{\Delta p}[-\bar{\omega}_{\mathrm{m}}(\bar{q}_2 - \bar{q}_1) - \bar{\omega}_{\mathrm{e}}(\bar{q}_{\mathrm{e}} - \bar{q}_2)]; \tag{3}$$

and δ_1 and δ_2 are SST-dependent heating switch-on coefficients (Wang and Li, 1994; Li, 2006),

$$\delta_1(\delta_2) = \begin{cases} 1, & \text{if SST} > 29.5, \text{and } Q_{\mathrm{m}}(\bar{Q}_{\mathrm{m}}) > 0 \\ (\text{SST} - 26.5)/3, & \text{if } 26.5 < \text{SST} < 29.5, \text{and } Q_{\mathrm{m}}(\bar{Q}_{\mathrm{m}}) > 0 \\ 0, & \text{if SST} < 26.5, \text{or } Q_{\mathrm{m}}(\bar{Q}_{\mathrm{m}}) < 0 \end{cases}. \tag{4}$$

In Eqs. (2) and (3), Δp (= 400 hPa) is the mean depth between the upper and lower free-atmosphere levels, and $\bar{q}_1$, $\bar{q}_2$, and $\bar{q}_{\mathrm{e}}$ represent mean specific humidity at the upper level, lower level, and in the boundary layer, respectively. The basic-state humidity fields are the function of specific humidity at the surface, and decay exponentially with height (Wang, 1988). Variables ω'_{m} and ω'_{e} denote vertical velocities in the middle troposphere and at the top of PBL respectively, while $\bar{\omega}_{\mathrm{m}}$ and $\bar{\omega}_{\mathrm{e}}$ denote summer mean vertical velocities at the middle level and the top of PBL respectively. In addition, b (= 0.9) is a fraction parameter measuring the efficiency of precipitation, and L_{c} is the latent heat of condensation per unit mass.

Although simple, this model contains essential dynamics and physics for tropical low-frequency motion (Wang and Li, 1994). The specified basic-state fields include geopotential height, wind, sea surface temperature (SST), and surface specific humidity derived from the NCEP/DOE Reanalysis II. By integrating the model forward, one may examine the temporal evolution of initial perturbation under the specified background mean state and structure and evolution characteristics of the most unstable mode simulated by the model.

3. Origins of the QBWO and ISO modes

We first reveal strong convective activity centers over the Asian monsoon domain. Figure 1a shows the standard deviation of the daily OLR field during May–October. As one can see, there are two major activity centers, with one over the SCS/western North Pacific (WNP) and the other over the BoB. The maximum value of the OLR standard deviation in the two regions exceeds 45 W m^{-2}.

The power spectrum analysis of the OLR anomaly averaged over the SCS (10°–20°N, 110°–120°E) reveals two dominant peaks on the quasi-biweekly (10–20-day) and intraseasonal (20–80-day) periods respectively (Fig. 1b). This result is consistent with many previous studies over the different tropical regions (e.g., Lau et al., 1988; Chen et al., 2000). The similar two power spectrum peaks are also seen over the BoB (10°–20°N, 85°–95°E) (figure omitted).

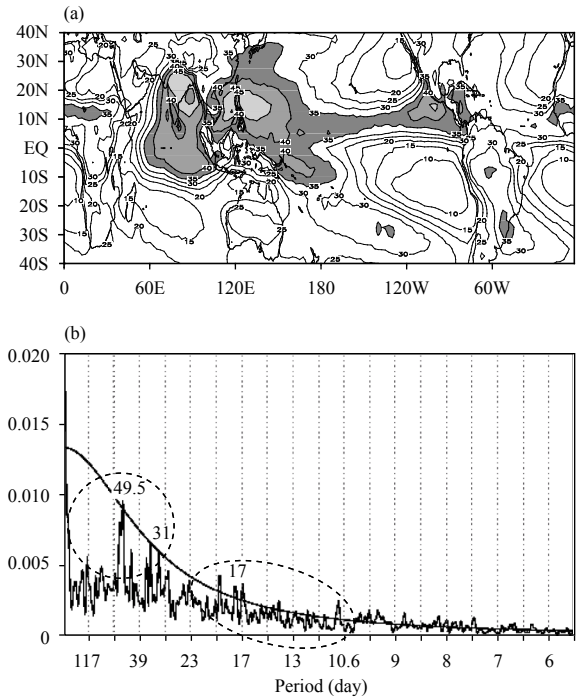

Fig. 1. (a) Standard deviation of boreal summer (May–October) daily OLR field during 1979–2001, with shadings representing values greater than 35 W m^{-2}. (b) Power spectrum of the OLR anomaly averaged over 10°–20°N, 110°–120°E, with the circle denoting the ISO band and the oval the QBWO band, and the solid line representing the lower bound of the 95% confidence interval.

To reveal the relative strength of the QBWO and ISO modes, a specially designed sharp bandpass filter (Christiano and Fitzgerald, 2003; also see Li et al., 2006) was applied to the daily OLR anomaly field, to separate the 10–20-day and 20–80-day modes. Figure 2 illustrates the standard deviations and the propagation vectors of the 10–20-day and 20–80-day filtered OLR fields. Note that strong OLR variabilities appear over both the SCS and BoB regions for both the QBWO and ISO modes. For example, the standard deviation of the OLR anomaly exceeds 20 W m^{-2} for the QBWO mode and 24 W m^{-2} for the ISO mode over the SCS. In general, the variabilities of the two modes are comparable and each accounts for approximately 50% of the total low-frequency variability.

Given the strong OLR variabilities over the SCS and BoB regions on both timescales, one may wonder what the origins of these variabilities are. Figure 2 shows that for the ISO mode, there is pronounced northward propagation of convection over the tropical Indian Ocean, SCS, and western Pacific, while the QBWO mode is dominated by westward or northwestward propagation.

A lagged correlation analysis with reference to the SCS box was performed and the results (Fig. 3) show that for the QBWO mode, convective signals originate in

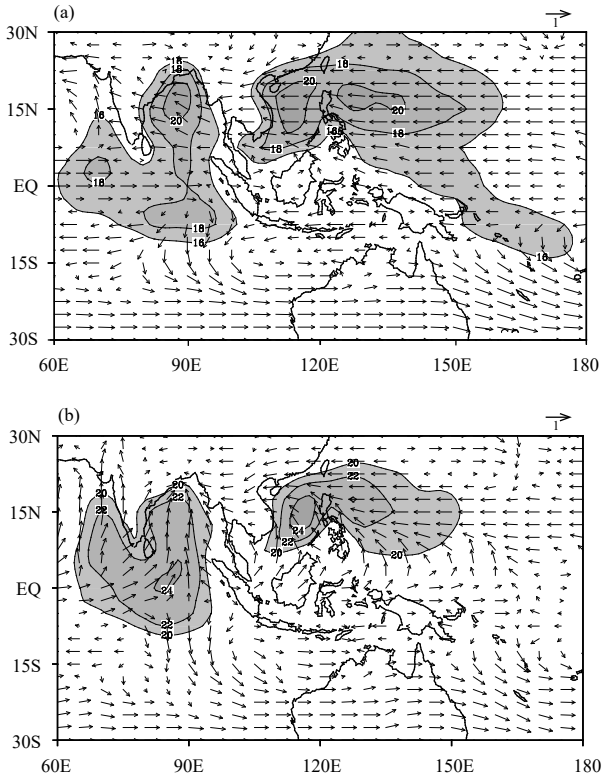

Fig. 2. Standard deviation (shading; W m^{-2}) and propagation vectors of the (a) 10–20-day and (b) 20–80-day filtered OLR fields.

the off-equatorial western Pacific and propagate westward into the SCS region. This is in contrast to the ISO mode in which convective signals originate from the equatorial Indian Ocean, propagate eastward along the equatorial Indian Ocean, and bifurcate toward the north after passing Sumatra. Such a feature is consistent with that found by Jiang et al. (2004) and Jiang and Li (2005).

A similar correlation analysis was carried out with reference to the BoB box (Fig. 4). Again, for the 10–20-day oscillation, the convective signal originates from the tropical western Pacific. For the 20–80-day mode, the major convective center moves eastward along the equatorial Indian Ocean, and then shifts northward after approaching the western coast of Sumatra.

Another way to show the dominant structure and propagation characteristics of the QBWO mode is through an EOF analysis. Before conducting EOF analysis, a 10–20-day bandpass filtering was applied to the original reanalysis fields. Then we calculated lagged correlation between principal components (PCs) of the first two leading EOF modes, and found that they have a significant maximum correlation at a 90-degree phase lag, suggesting that they represent the same physical mode.

Figure 5 illustrates the evolution of the 850-hPa wind and vorticity fields associated with the QBWO mode from day 0 to 3 based on the EOF analysis above. Here day 0 corresponds to the time when maximum vorticity appears at 10°N, 140°E. A northwest–southeast oriented wave train pattern, with a total horizontal wavelength of about 4000 km, appears over the WNP. The corresponding zonal wavelength is about 6000 km. The wave train propagates northwestward, similar to the convective anomaly shown in the left panels of Fig. 3.

The result above points out the different origins of the 10–20- and 20–80-day oscillations over the SCS and BoB. The convective signals associated with the QBWO mode originate from off-equatorial western Pacific, whereas the convective signals associated with the ISO mode originate from the equatorial Indian Ocean. An important science question is why the off-equatorial mode favors a 10–20-day period while the equatorial mode prefers a 20–80-day period.

We hypothesize that such a difference lies on distinctive wave dynamics and circulation patterns between equatorial and off-equatorial regions. At the equator, because of vanished Coriolis force, divergent vertical overturning circulations and equatorial Kelvin waves dominate. As a result, a planetary zonal scale (i.e., a wavelength of 36,000 km) is selected. Off the equator, rotational circulations and Rossby waves dominate. As a result, a wave train pattern with alternated cyclone and anticyclone structure is excited. The off-equatorial wave train has a typical zonal wavelength of about 6000 km (Fig. 5). Given that the ratio of phase speed of Rossby wave versus Kelvin wave is about one-third (Matsuno, 1966), and ratio of the zonal wavelength of the off-equatorial mode versus that of the equatorial mode is about one-sixth, the time period that an equatorial perturbation takes to travel over one wavelength is about two times as large as that of an off-equatorial perturbation. This explains why the period of the equatorial mode is longer than that of the off-equatorial mode.

The discussion above is based on physical argument. Here the spatial scales for the equatorial and off-equatorial modes are derived from the observations (e.g., Wang and Rui, 1990; Hsu and Weng, 2001). In the following, we intend to demonstrate the spatial and temporal scale selection for the two modes based on a simple atmospheric model.

4. Temporal and spatial scale selection of off-equatorial and equatorial modes in a simple theoretical model

A 2.5-layer atmospheric model was applied in Li and Zhou (2009) to investigate the scale selection of the

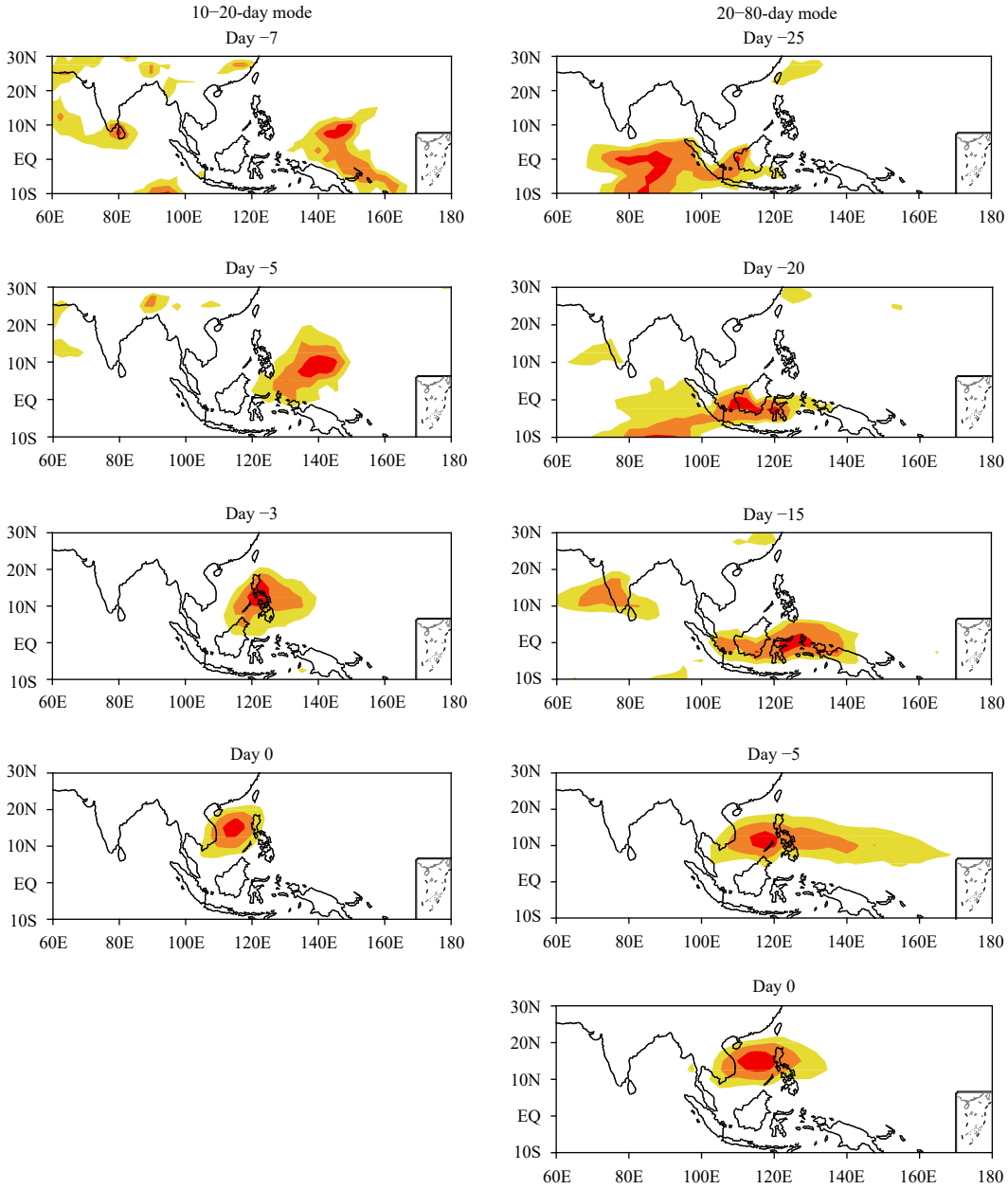

Fig. 3. Lagged correlation (shading; values: 0.5, 0.7, 0.9) maps of the OLR anomaly fields associated with boreal summer QBWO (left; from day –7 to day 0) and ISO (right; from day –25 to day 0) modes. The correlation was done based on the reference point over the South China Sea (SCS) box (10°–20°N, 110°–120°E). It has been normalized by the maximum correlation coefficient in each panel.

equatorial mode. It was found that atmospheric nonlinear heating is crucial for the planetary scale selection of the equatorial mode. Figure 6 shows simulated zonal wind anomaly at the equator for an initial wavenumber-5 perturbation case. During the first 10-day integration, the perturbation remains the initial wavenumber structure, as it moves eastward along the equator. After an adjustment period, the amplitude of the initial wavenumber-5 perturbation decays rapidly, while a wavenumber-1 perturbation emerges and develops. By day 20, the zonal wind at the equator is dominated by a wavenumber-1 zonal structure.

Numerical experiments with other initial wavenumber perturbation cases (from wavenumber 1 to 15) show the essentially same final solution (Li and Zhou, 2009). Therefore, regardless of what initial perturbations are given, the nonlinear heating causes a final scale selection at planetary zonal scale. The horizontal structure of this most unstable mode shows a Kelvin–Rossby wave couplet pattern (Li and Wang, 1994; Wang and Li, 1994), which is similar to the observed (see Hendon and Salby, 1994). The estimated zonal phase speed in the

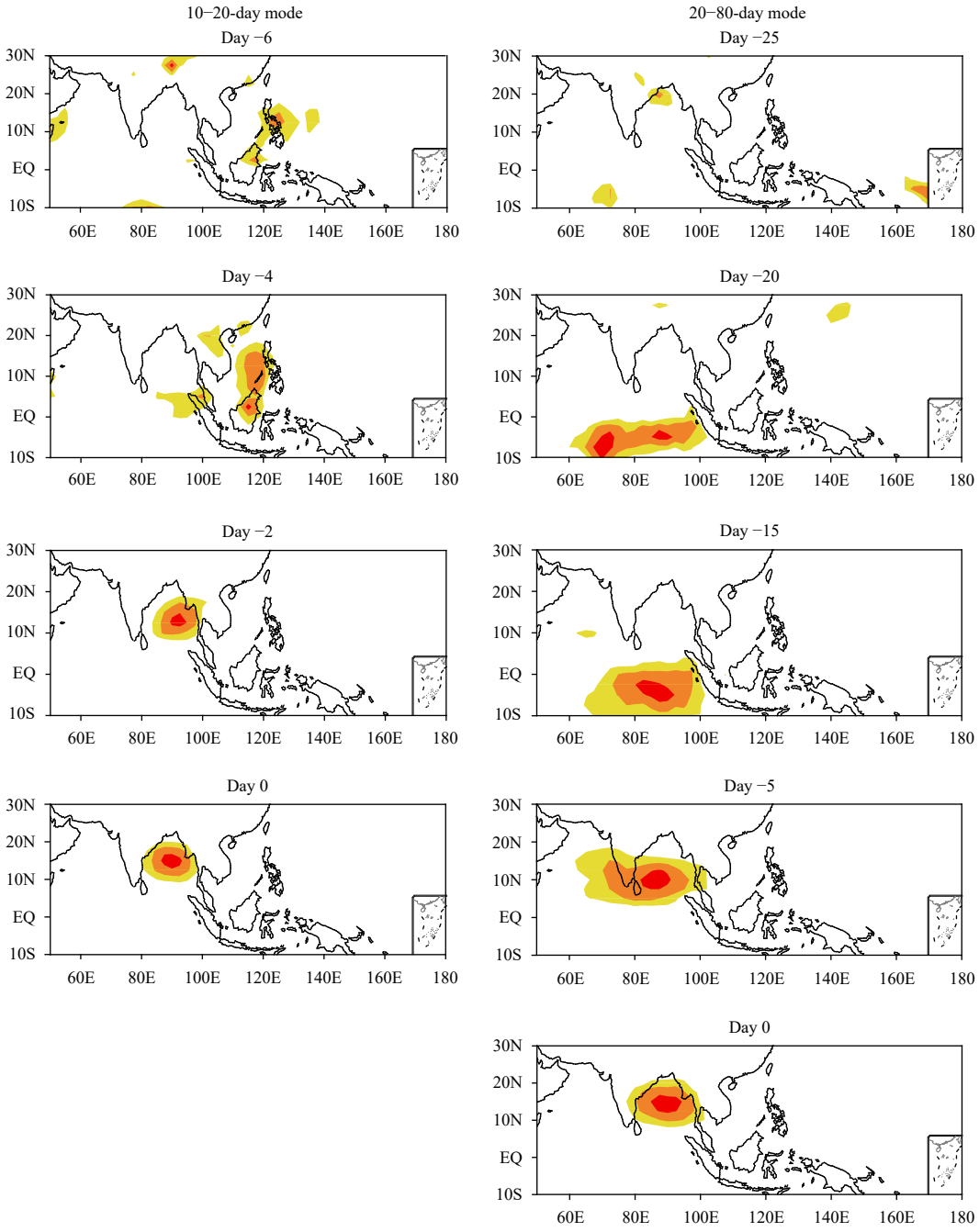

Fig. 4. As in Fig. 3, except for the reference point over the Bay of Bengal (BoB) box (10°–20°N, 85°–95°E).

model is about 12 degrees per day, which corresponds to a period of 30 days to circulate around the globe. This simulated period is well within the intraseasonal range.

The numerical model result above indicates that the equatorial mode favors the most unstable growth at planetary zonal scale and a preferred period of 20–80 days in general. Following this approach, we intend to examine the temporal and spatial scale selection dynamics of the off-equatorial mode, using the same atmospheric model. To focus on examining the off-equatorial mode, a strong dynamic/thermodynamic damping (1×10^{-4} s^{-1}) is applied to the regions north of 30°N and south of 5°N. Within 5°–30°N, a modest dynamic/thermodynamic damping coefficient of 2×10^{-6} s^{-1} is applied, which corresponds to an *e*-folding timescale of approximately 5 days.

It is hypothesized that the QBWO is the most unstable mode under the summer mean flow over the off-equatorial Indo–western Pacific warm pool. To test this hypothesis, we design a number of numerical experiments using the

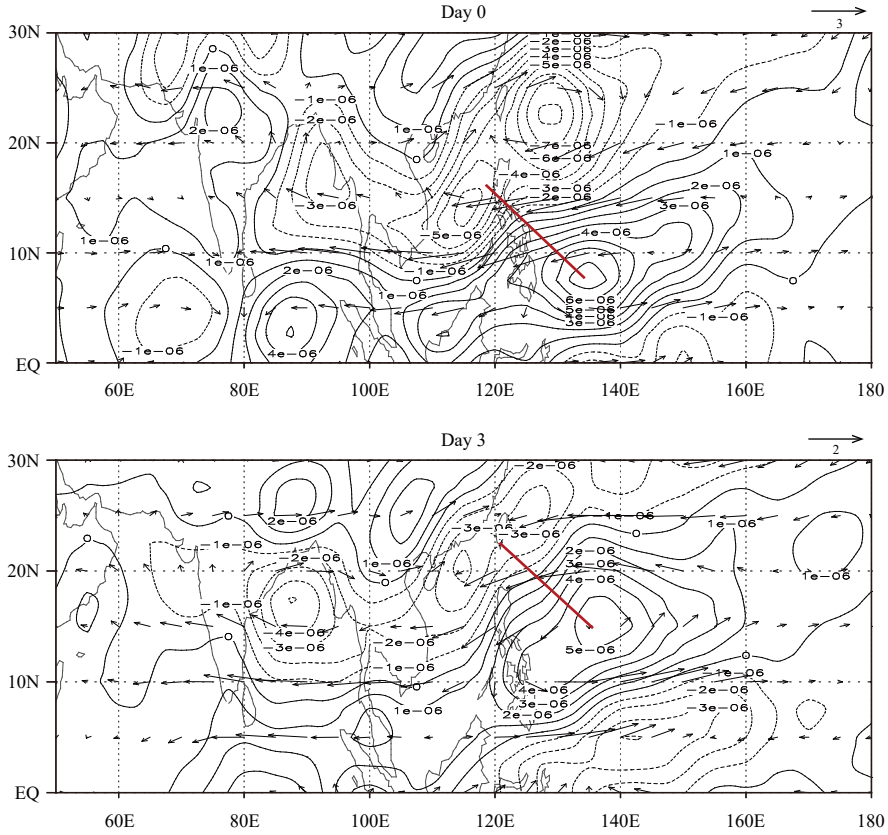

Fig. 5. Evolution of 850-hPa wind (vector; m s^{-1}) and vorticity (contour; s^{-1}) fields associated with the QBWO mode from day 0 (upper) to 3 (lower panel) in boreal summer, derived based on the time-lag composite of the leading EOF modes. Red line represents a half of horizontal wavelength.

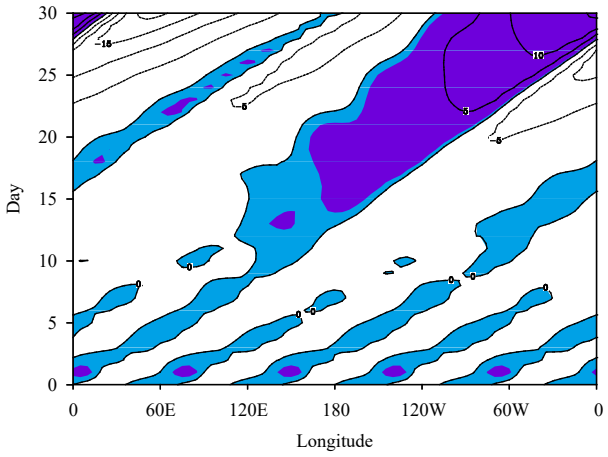

Fig. 6. Time–longitude section of the equatorial zonal wind in the lower troposphere from the 2.5-layer model simulation under the nonlinear heating. An initial wavenumber-5 perturbation was introduced. The contour interval is 5 m s^{-1} and the shading represents the westerly wind. From Li and Zhou (2009).

2.5-layer atmospheric model. Our strategy is to introduce a weak vorticity perturbation initially with different zonal wavenumbers and examine how the perturbation grows with time and what the structure and propagation characteristics of the most unstable mode simulated by the model are.

The observed three-dimensional summer mean fields are specified as the model basic state. The mean circulation over the monsoon trough region is characterized by low-level convergence, cyclonic vorticity, ascending motion, easterly vertical shear, and high mean SST and moisture content. These dynamic and thermodynamic conditions favor the growth of tropical disturbances.

The initial perturbations have the form of an off-equatorial Rossby wave centered at 16°N, with a zonal wavenumber ranging from 1 to 20. The initial perturbation stream function (ψ) has its maximum amplitude at the central latitude (16°N) and decreases to zero at 6° and 26°N. The perturbation zonal and meridional winds are then derived from the stream function field: $u = -\dfrac{\partial \psi}{\partial y}$ and $v = \dfrac{\partial \psi}{\partial x}$. The initial perturbation geopotential height field is given by $\Phi = f\psi$ according to the quasi-geostrophic approximation. Figure 7 shows the initial geopotential height and wind fields for zonal wavenumber 3 at the lower free-atmospheric level. A high (low) pressure is

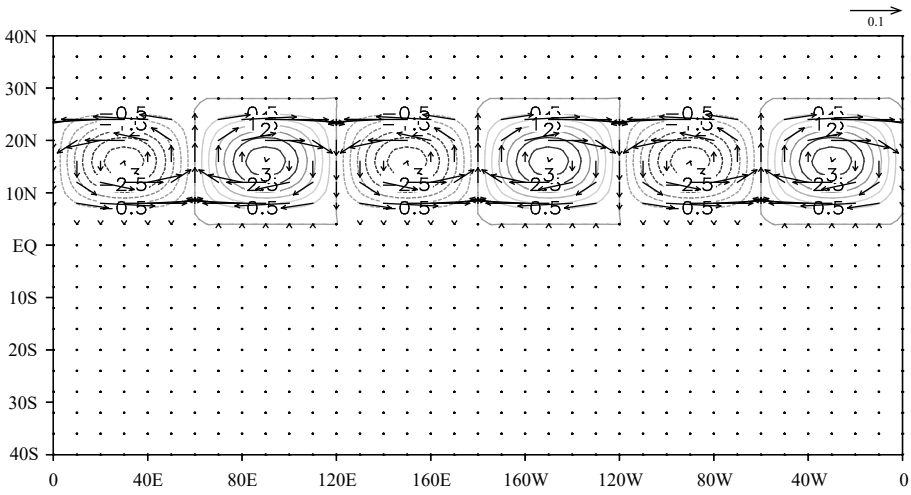

Fig. 7. Initial perturbation fields of wavenumber-3 geopotential height (contour; $m^2\ s^{-2}$) and wind (vector; $m\ s^{-1}$) at 850 hPa.

collocated with the anticyclonic (cyclonic) circulation in the Northern Hemisphere. For other initial perturbations, only the zonal wavenumber varies while the structure and amplitude remain the same.

The numerical simulations indicate that regardless of what initial zonal wavenumbers are given, the structure and propagation characteristics of the model final solutions are always the same. Figure 8 illustrates the normalized (divided by the maximum amplitude at each time level) low-level vorticity fields at day 14 for initial zonal wavenumber 1 (upper panel), 5 (middle panel), and 9 (lower panel) cases. Note that a northwest–southeast oriented wave train is simulated in each experiment. The wave train has a typical total wavelength of about 4000 km (or a zonal wavelength of approximately 6000 km), consistent with the observational diagnosis (Fig. 5). The maximum perturbation appears in the region of strong background easterly shear and high mean SST and specific humidity.

To illustrate the evolution characteristic of the most unstable mode, Fig. 9 shows the time sequence of the normalized vorticity field at day 15 (upper panel), 16 (middle panel), and 17 (lower panel) for initial zonal wavenumber 5 case. It is seen that the wave train propagates northwestward at a phase speed of approximately 5 degrees per day. The northwestward propagation is robust for all cases with different initial zonal wavenumbers. Another noted feature is the low-frequency growth of the perturbations—the amplitudes of the vorticity perturbation increase from day 15 to day 17 (from 4.5×10^{-6} s^{-1} to 5.4×10^{-6} s^{-1}).

The zonal phase propagation speed may be estimated based on the time–longitude section of the normalized vorticity field from day 14 to day 17 (Fig. 10). Our calcu-

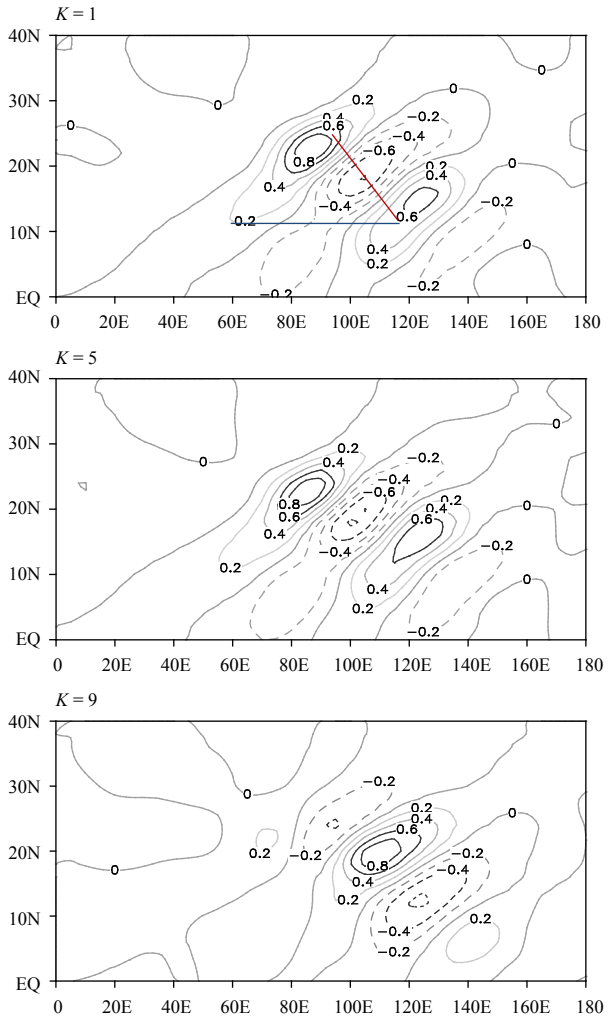

Fig. 8. Simulated low-level vorticity fields at day 14 for initial zonal wavenumber 1 (upper), 5 (middle), and 9 (lower panel) cases. The vorticity field in each panel has been normalized by its amplitude to clearly illustrate the horizontal wave train pattern. Red line represents the total horizontal wavelength and blue line represents the zonal wavelength.

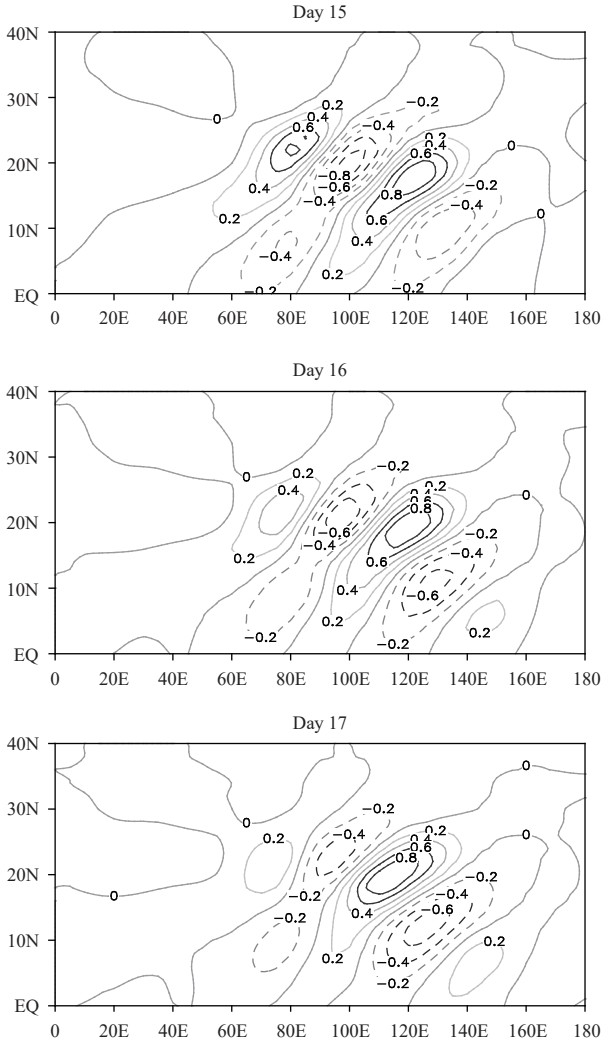

Fig. 9. Evolution of the normalized low-level vorticity field at day 15 (upper), 16 (middle), and 17 (lower panel) for the initial zonal wavenumber 5 case. The maximum amplitudes of the vorticity from day 15 to 17 are 4.5×10^{-6} s^{-1}, 4.9×10^{-6} s^{-1}, and 5.4×10^{-6} s^{-1}, respectively.

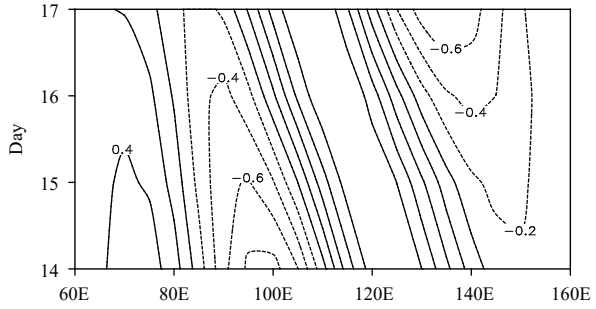

Fig. 10. Time–longitude section of the normalized low-level vorticity field from day 14 to day 17 for the initial zonal wavenumber 5 case.

lation shows that the westward zonal phase speed is at the range of 3–6 m s^{-1}. At a fixed location, one may estimate the period of the off-equatorial mode based on its zonal wavelength and zonal phase speed. For a zonal wavelength of 6000 km and a zonal phase speed of 3–6 m s^{-1}, the corresponding period is about 10–20 days.

The dependence of the zonal wavelength and period of the most unstable mode in the off-equatorial region on the initial zonal wavenumber is plotted in Fig. 11. It shows that they are insensitive to the initial wavelength. The result implies that the QBWO is an intrinsic atmospheric mode in boreal summer over the off-equatorial Indo–western Pacific warm pool region.

What causes the northwestward propagation of the wave train? Jiang et al. (2004) and Drbohlav and Wang (2005) suggested that the basic-state easterly shear contributes to the northward propagation through the generation of the free-atmospheric barotropic vorticity and PBL convergence ahead of the convection. Thus, the combination of the β effect and the vertical shear effect may lead to the northwestward propagation. Li (2006) demonstrated that the tropical perturbation grows at a faster rate under an easterly shear than a westerly shear. Figure 12 shows the spatial phase relationship between the PBL divergence and mid-tropospheric vertical motion. Note that the PBL convergence (divergence) slightly leads the mid-tropospheric ascending (descending) motion, consistent with the observational analysis result (Hsu and Weng, 2001). Such a phase shift favors the northwestward

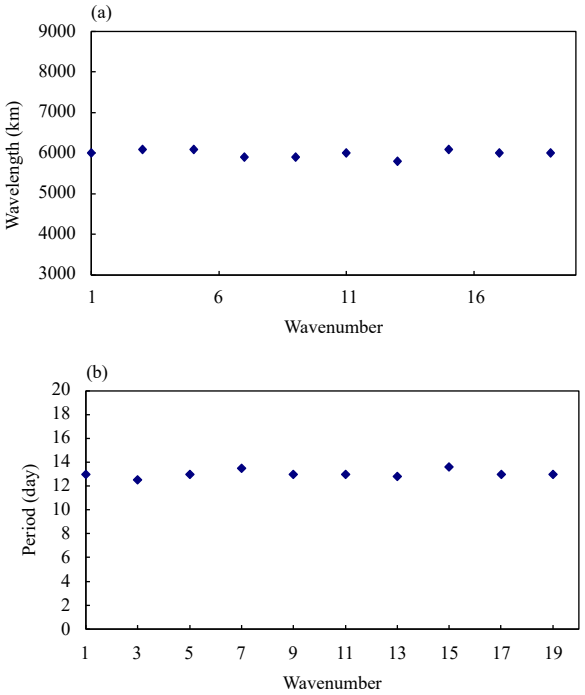

Fig. 11. (a) Zonal wavelength (vertical axis) and (b) period of the final model solution as a function of initial zonal wavenumber (zonal axis) ranging from 1 to 20.

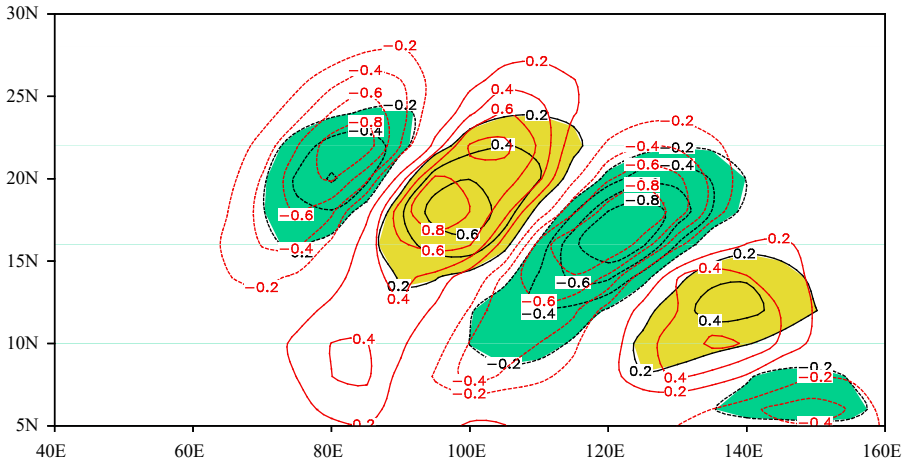

Fig. 12. The mid-tropospheric vertical *p*-velocity (shading and black contours) and the PBL divergence (red contours) at day 15 obtained from the initial zonal wavenumber 5 case. Both the vertical velocity and the PBL divergence fields have been normalized by their maximum amplitudes to clearly see their horizontal structures.

propagation because the PBL convergence increases the low-level moisture and favors the development of a convectively unstable stratification (Hsu and Li, 2012). Such a phase relation is also found in other simulations with different initial wavenumbers.

In the control experiments above, the observed summer mean flow is specified as the model basic state. Is the summer mean flow crucial in generating the northwest–southeast oriented QBWO mode? To address this question, a sensitivity test was conducted by removing the summer mean flow (i.e., specifying a resting environment) while keeping the same SST and surface humidity fields. Figure 13 shows the simulated low-level vorticity field under the resting environment condition. For all the zonal wavenumber cases, only one primary vorticity center is found, and there is no clear northwest–southeast oriented wave train pattern. Furthermore, the maximum vorticity center appears quasi-stationary and there is no northwestward propagation. Thus, this sensitivity experiment demonstrates the importance of the summer mean flow in generating the QBWO mode in the off-equatorial region.

The initial perturbations specified in all the previous experiments have the form of Rossby waves. To examine the sensitivity of the model solution to the initial perturbation type, we conducted the second set of sensitivity experiments, in which initial perturbations are specified in the form of equatorial Kelvin waves, as shown in Fig. 14. In this case, the maximum amplitude of the initial perturbation is located at the equator, with high (low) pressure anomalies being collocated with westerly (easterly) anomalies.

Despite of this very different initial condition, the

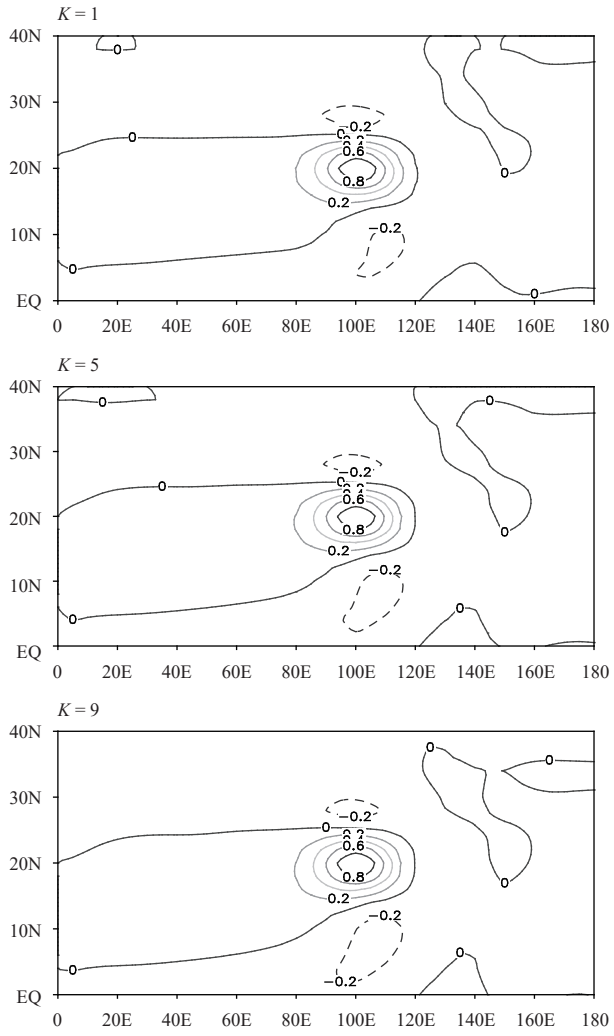

Fig. 13. Normalized low-level vorticity fields at day 25 for initial zonal wavenumber 1 (upper), 5 (middle), and 9 (lower panel) cases under a resting environment. Same initial perturbations as in Fig. 7 were specified.

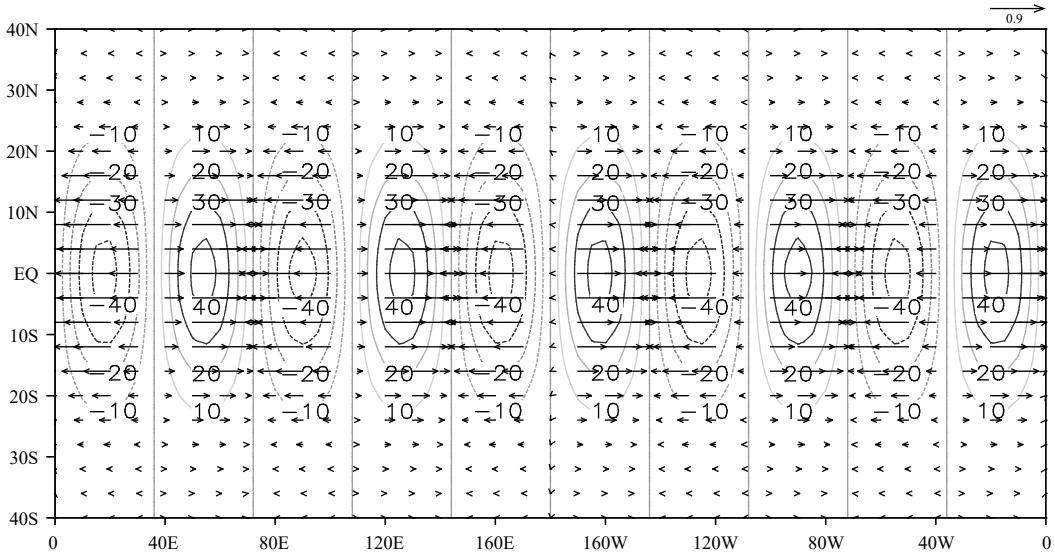

Fig. 14. Horizontal distribution of an initial wavenumber-5 perturbation that has a form of equatorial Kelvin wave (vector: low-level wind, m s^{-1}; contour: low-level geopotential height, m^2 s^{-2}).

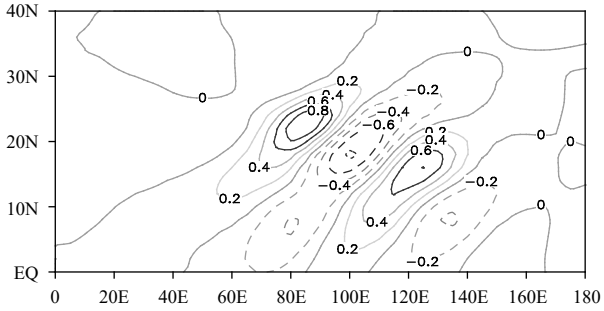

Fig. 15. Normalized low-level vorticity field simulated by the model at day 14, with the initial condition shown in Fig. 14.

model final solution is a northwest–southeast oriented wave train pattern (Fig. 15), identical to that in the control experiments. The result again confirms that the QBWO mode results from the instability of the summer mean flow in the presence of convection–circulation feedback. Regardless of what initial condition is, the final solution of the unstable mode is always the northwest–southeast oriented wave train pattern with a zonal wavelength of about 6000 km and a period of about 10–20 days, propagating northwestward.

5. Conclusions and discussion

The observational analysis of daily OLR field shows two significant power spectrum peaks at 10–20- and 20–80-day periods over the SCS and BoB. By separating the two timescale components, we found that the quasi-biweekly oscillation over both the regions originates from the off-equatorial western North Pacific, with pronounced northwestward propagation. The origin of the 20–80-day mode in the BoB and SCS, on the other hand, is the equatorial Indian Ocean. The convective signals associated with the 20–80-day mode propagate eastward and northward over the Indo–Pacific warm pool region.

The observational analysis result above suggests that the equatorial mode prefers a 20–80-day period, while the off-equatorial mode prefers a 10–20-day period. The cause of such a scale selection is further explored through a simple 2.5-layer linear atmospheric model. The numerical model experiments show that regardless of what initial perturbations are given, under the boreal summer mean flow, the model simulates the most unstable mode in the off-equatorial region that is characterized by a northwest–southeast oriented wave train pattern with a typical zonal wavelength of about 6000 km, propagating northwestward. The maximum growth of the perturbation appears in the region of the strong background easterly vertical shear and high mean SST/surface moisture. The wave train propagates northwestward at a phase speed of 3–6 m s^{-1}. For a fixed observer, a zonal wavelength of 6000 km and a phase speed of 3–6 m s^{-1} correspond to a period of about 10–20 days.

While the focusing region is the equatorial zone, the model simulates an MJO like disturbance that has a Kelvin–Rossby wave couplet structure, propagating eastward along the equator. The equatorial disturbance has a preferred wavenumber-1 zonal structure, with a typical period at the range of 20–80 days.

Thus, the numerical model experiments confirm the distinctive temporal and spatial scale selections for the

equatorial and off-equatorial modes. The QBWO is an intrinsic atmospheric mode over the off-equatorial western Pacific in the presence of the summer mean flow. Its structure resembles the form of Rossby waves with a typical zonal wavelength of 6000 km and a period of 10–20 days. This is distinctive from the MJO-like mode at the equator that has a dominant planetary zonal scale and a 20–80-day period.

It is worth mentioning that while the current simple model simulates a preferred northwest–southeast oriented wave train with a horizontal wavelength around 4000 km, a study by Li (2006) using a different model reproduced a wave train pattern in western North Pacific that has a typical wavelength of 2500 km. Given the similar summer mean state specified, one may wonder what causes the difference. We speculate that it might be caused by different treatments of governing equations and heating parameterization. In Li (2006), a global atmospheric general circulation model was used. The model consists of primitive governing equations with a spectrum dynamic core and five vertical levels. The heating in the model is proportional to perturbation vorticity in the lower troposphere. In the current model, the governing equations are simplified in such a way that only the first baroclinic mode is considered in the free atmosphere, and the heating is proportional to boundary layer and lower tropospheric moisture convergence. The exact cause of the different solutions between the two models is unclear at the moment. A further in-depth study is needed to understand the difference.

It is also worth mentioning that in a linear model like the one used here, only the most unstable mode can be seen in the final solution (other modes are too weak to be detected). This is why in the off-equatorial mode simulations a strong damping is applied in the equatorial zone and in the midlatitude region. By doing so one may focus on the structure and evolution characteristics of the off-equatorial mode. The MJO-like equatorial mode, on the other hand, can be easily stimulated in a tropical channel model under either a resting environment or a realistic summer or winter mean state.

REFERENCES

Chatterjee, P., and B. N. Goswami, 2004: Structure, genesis and scale selection of the tropical quasi-biweekly mode. *Quart. J. Roy. Meteor. Soc.*, **130**, 1171–1194, doi: 10.1256/qj.03.133.

Chen, T.-C., M.-C. Yen, and S.-P. Weng, 2000: Interaction between the summer monsoons in East Asia and the South China Sea: Intraseasonal monsoon modes. *J. Atmos. Sci.*, **57**, 1373–1392, doi: 10.1175/1520-0469(2000)057<1373:IBTSMI>2.0.CO;2.

Christiano, L. J., and T. J. Fitzgerald, 2003: The band pass filter. *Int. Econ. Rev.*, **44**, 435–465, doi: 10.1111/1468-2354.t01-1-00076.

Drbohlav, H.-K. L., and B. Wang, 2005: Mechanism of the northward-propagating intraseasonal oscillation: Insights from a zonally symmetric model. *J. Climate*, **18**, 952–972, doi: 10.1175/JCLI3306.1.

Goswami, P., and V. Mathew, 1994: A mechanism of scale selection in tropical circulation at observed intraseasonal frequencies. *J. Atmos. Sci.*, **51**, 3155–3166, doi: 10.1175/1520-0469(1994)051<3155:AMOSSI>2.0.CO;2.

Hendon, H. H., and M. L. Salby, 1994: The life cycle of the Madden–Julian oscillation. *J. Atmos. Sci.*, **51**, 2225–2237, doi: 10.1175/1520-0469(1994)051<2225:TLCOTM>2.0.CO;2.

Hsu, H.-H., and C.-H. Weng, 2001: Northwestward propagation of the intraseasonal oscillation in the western North Pacific during the boreal summer: Structure and mechanism. *J. Climate*, **14**, 3834–3850, doi: 10.1175/1520-0442(2001)014<3834:NPOTIO>2.0.CO;2.

Hsu, P.-C., and T. Li, 2012: Role of the boundary layer moisture asymmetry in causing the eastward propagation of the Madden–Julian oscillation. *J. Climate*, **25**, 4914–4931, doi: 10.1175/JCLI-D-11-00310.1.

Jiang, X.-A., and T. Li, 2005: Reinitiation of the boreal summer intraseasonal oscillation in the tropical Indian Ocean. *J. Climate*, **18**, 3777–3795, doi: 10.1175/JCLI3516.1.

Jiang, X. N., T. Li, and B. Wang, 2004: Structures and mechanisms of the northward propagating boreal summer intraseasonal oscillation. *J. Climate*, **17**, 1022–1039, doi: 10.1175/1520-0442(2004)017<1022:SAMOTN>2.0.CO;2.

Kanamitsu, M., W. Ebisuzaki, J. Woollen, et al., 2002: NCEP–DOE AMIP-II Reanalysis (R-2). *Bull. Amer. Meteor. Soc.*, **83**, 1631–1644, doi: 10.1175/BAMS-83-11-1631.

Lau, K.-M., G. J. Yang, and S. H. Shen, 1988: Seasonal and intraseasonal climatology of summer monsoon rainfall over East Asia. *Mon. Wea. Rev.*, **116**, 18–37, doi: 10.1175/1520-0493(1988)116<0018:SAICOS>2.0.CO;2.

Li, C. H., T. Li, A. L. Lin, et al., 2015: Relationship between summer rainfall anomalies and sub-seasonal oscillations in South China. *Climate Dyn.*, **44**, 423–439, doi: 10.1007/s00382-014-2172-y.

Li, T., 2006: Origin of the summertime synoptic-scale wave train in the western North Pacific. *J. Atmos. Sci.*, **63**, 1093–1102, doi: 10.1175/JAS3676.1.

Li, T., 2014: Recent advance in understanding the dynamics of the Madden–Julian oscillation. *J. Meteor. Res.*, **28**, 1–33, doi: 10.1007/s13351-014-3087-6.

Li, T., and B. Wang, 2005: A review on the western North Pacific monsoon: Synoptic-to-interannual variabilities. *Terr. Atmos. Oceanic Sci.*, **16**, 285–314, doi: 10.3319/TAO.2005.16.2.285(A).

Li, T., and C. H. Zhou, 2009: Planetary scale selection of the Madden–Julian oscillation. *J. Atmos. Sci.*, **66**, 2429–2443, doi: 10.1175/2009JAS2968.1.

Li, T., and P.-C. Hsu, 2018: *Fundamentals of Tropical Climate Dynamics*. Springer, Cham, 229 pp, doi: 10.1007/978-3-319-59597-9.

Li, T., P. Liu, X. Fu, et al., 2006: Spatiotemporal structures and mechanisms of the tropospheric biennial oscillation in the

Indo-Pacific warm ocean regions. *J. Climate*, **19**, 3070–3087, doi: 10.1175/JCLI3736.1.

Li, T., L. Wang, M. Peng, et al., 2018: A paper on the tropical intraseasonal oscillation published in 1963 in a Chinese journal. *Bull. Amer. Meteor. Soc.*, **99**, 1765–1779, doi: 10.1175/BAMS-D-17-0216.1.

Li, T. M., and B. Wang, 1994: The influence of sea surface temperature on the tropical intraseasonal oscillation: A numerical study. *Mon. Wea. Rev.*, **122**, 2349–2362, doi: 10.1175/1520-0493(1994)122<2349:TIOSST>2.0.CO;2.

Madden, R. A., and P. R. Julian, 1971: Detection of a 40–50 day oscillation in the zonal wind in the tropical Pacific. *J. Atmos. Sci.*, **28**, 702–708, doi: 10.1175/1520-0469(1971)028<0702:DOADOI>2.0.CO;2.

Madden, R. A., and P. R. Julian, 1972: Description of global-scale circulation cells in the tropics with a 40–50 day period. *J. Atmos. Sci.*, **29**, 1109–1123, doi: 10.1175/1520-0469(1972)029<1109:DOGSCC>2.0.CO;2.

Matsuno, T., 1966: Quasi-geostrophic motions in the equatorial area. *J. Meteor. Soc. Japan*, **44**, 25–43, doi: 10.2151/jmsj1965.44.1_25.

Murakami, T., 1980: Empirical orthogonal function analysis of satellite-observed outgoing longwave radiation during summer. *Mon. Wea. Rev.*, **108**, 205–222, doi: 10.1175/1520-0493(1980)108<0205:EOFAOS>2.0.CO;2.

Teng, H. Y., and B. Wang, 2003: Interannual variations of the boreal summer intraseasonal oscillation in the Asian–Pacific region. *J. Climate*, **16**, 3572–3584, doi: 10.1175/1520-0442(2003)016<3572:IVOTBS>2.0.CO;2.

Wang, B., 1988: Dynamics of tropical low-frequency waves: An analysis of the moist Kelvin wave. *J. Atmos. Sci.*, **45**, 2051–2065, doi: 10.1175/1520-0469(1988)045<2051:DOTLFW>2.0.CO;2.

Wang, B., and H. Rui, 1990: Synoptic climatology of transient tropical intraseasonal convection anomalies: 1975–1985. *Meteor. Atmos. Phys.*, **44**, 43–61, doi: 10.1007/BF01026810.

Wang, B., and T. M. Li, 1994: Convective interaction with boundary-layer dynamics in the development of a tropical intraseasonal system. *J. Atmos. Sci.*, **51**, 1386–1400, doi: 10.1175/1520-0469(1994)051<1386:CIWBLD>2.0.CO;2.

Wang, B., and X. S. Xie, 1997: A model for the boreal summer intraseasonal oscillation. *J. Atmos. Sci.*, **54**, 72–86, doi: 10.1175/1520-0469(1997)054<0072:AMFTBS>2.0.CO;2.

Wen, M., T. Li, R. H. Zhang, et al., 2010: Structure and origin of the quasi-biweekly oscillation over the tropical Indian Ocean in boreal spring. *J. Atmos. Sci.*, **67**, 1965–1982, doi: 10.1175/2009JAS3105.1.

Xie, Y.-B., S.-J. Chen, Y.-L. Zhang, et al., 1963: A preliminarily statistic and synoptic study about the basic currents over southeastern Asia and the initiation of typhoons. *Acta Meteor. Sinica*, **33**, 206–217, doi: 10.11676/qxxb1963.020. (in Chinese)

Xie, Y.-B., S.-J. Chen, Y.-L. Zhang, et al., 2018: A preliminarily statistic and synoptic study about the basic currents over southeastern Asia and the initiation of typhoons (English Edition). *J. Meteor. Res.*, **32**, 661–669, doi: 10.1007/s13351-018-8888-6.

Xu, Z. Q., T. Li, and K. Fan, 2017: The weakened intensity of the atmospheric quasi-biweekly oscillation over the western North Pacific during late summer around the late 1990s. *J. Climate*, **30**, 9807–9826, doi: 10.1175/JCLI-D-16-0759.1.

Tech & Copy Editor: Qi WANG